NANO LETTERS
Letter
Cite This: Nano Lett. 2019, 19, 7357−7364
pubs.acs.org/NanoLett

Probing Spatial Phonon Correlation Length in Post-Transition Metal Monochalcogenide GaS Using Tip-Enhanced Raman Spectroscopy

R. S. Alencar,*[,†,‡,§] Cassiano Rabelo,[∥] Hudson L. S. Miranda,[∥] Thiago L. Vasconcelos,[⊥] Bruno S. Oliveira,[⊥] Aroldo Ribeiro,[‡] Bruno C. Públio,[‡] Jenaina Ribeiro-Soares,[#] A. G. Souza Filho,[§] Luiz Gustavo Cançado,[‡] and Ado Jorio*[,‡]

[†]Faculdade de Física, Universidade Federal do Pará, 66075-110 Belém-PA, Brazil

[‡]Departamento de Física, Universidade Federal de Minas Gerais, Belo Horizonte, Minas Gerais 30270-901, Brazil

[§]Departamento de Física, Centro de Ciências, Universidade Federal do Ceará, P. O. Box 6030, Fortaleza, Ceará 60455-900, Brazil

[∥]Programa de Pós-Graduação em Engenharia Elétrica, Universidade Federal de Minas Gerais, Av. Antônio Carlos 6627, 31270-901 Belo Horizonte, MG, Brazil

[⊥]Divisão de Metrologia de Materiais, Instituto Nacional de Metrologia Qualidade e Tecnologia (INMETRO), Duque de Caxias, Rio de Janeiro 25250-020, Brazil

[#]Departamento de Física, Universidade Federal de Lavras, Lavras, Minas Gerais 37200-000, Brazil

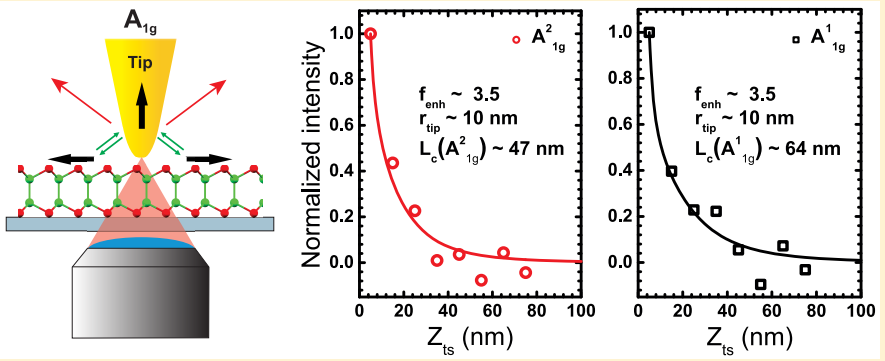

ABSTRACT: The knowledge of the phonon coherence length is of great importance for two-dimensional-based materials since phonons can limit the lifetime of charge carriers and heat dissipation. Here we use tip-enhanced Raman spectroscopy (TERS) to measure the spatial correlation length L_c of the A^1_{1g} and A^2_{1g} phonons of monolayer and few-layer gallium sulfide (GaS). The differences in L_c values are responsible for different enhancements of the A_{1g} modes, with A^1_{1g} always enhancing more than the A^2_{1g}, independently of the number of GaS layers. For five layers, the results show an L_c of 64 and 47 nm for A^1_{1g} and A^2_{1g}, respectively, and the coherence lengths decrease when decreasing the number of layers, indicating that scattering with the surface roughness plays an important role.

KEYWORDS: *GaS, tip-enhanced Raman spectroscopy, phonon coherence length, spatial correlation length*

Different transition metal di- and monochalcogenides, all together generate an important family of materials that cover a range of properties for functional devices.[1,2] The metal monochalcogenide GaS is a layered two-dimensional (2D) semiconductor with an indirect (direct) band gap of 2.5 eV (3.0 eV),[3−6] promising for future applications in photoelectric devices, electrical sensors, and nonlinear optical applications[7] because of its out-of-plane anisotropic structural, electrical, optical and mechanical properties. Each GaS monolayer is formed by two planes of sulfur (S) atoms sandwiching two planes of gallium (Ga) atoms linked via covalent bonds and stacked along the *C*-axis to build up the bulk GaS.[3]

Phonons play a crucial role in optical, electrical, and thermal transport of materials. Particularly, scattering by optical phonons has been observed to limit electrical transport and heat dissipation,[8−10] so that the knowledge of phonon spatial coherence in GaS is important for electronics application, specially in the nanoscale domain, where phonon interference becomes increasingly significant.[11]

Raman spectroscopy is a powerful technique for studying 2D systems, being extensively used in the characterization of the number of layers,[12,13] defects,[14,15] doping,[16−18] stoichiometry,[6,19] optical and mechanical properties of those systems,[20−25] although the majority of the studies are limited to microscopic scale imposed by the light diffraction limit. TERS-based subdiffraction investigations[26,27] of 2D systems have

Received: July 20, 2019
Revised: August 25, 2019
Published: August 30, 2019

DOI: 10.1021/acs.nanolett.9b02974
Nano Lett. 2019, 19, 7357−7364

been mainly dedicated to graphene and transition metal dichalcogenides (TDMs).[28−36]

For graphene, TERS has been commonly used to probe local properties, such as defects (point defects,[34] linear defects,[36] and grain boundaries[33,37]), surface contamination,[38,39] strain,[35,40−43] and doping.[16] Interestingly, it has been demonstrated that phonons with different symmetries in graphene exhibit different tip-induced enhancement due to near-field interference effects, which are not present in microscopic (far-field) spectroscopy.[36,44,45] Here we show that this same effect can be used to measure distinct phonon coherence lengths for phonons belonging to the same symmetry. In this sense, GaS is special for having two distinct totally symmetric Raman-active optical phonons, and we here use TERS to probe the spatial correlation length of optical phonons belonging to the A_{1g} irreducible representation in GaS.

We present here a TERS investigation of the optical properties of GaS with different thicknesses. The different enhancements of the two A_{1g} modes are then attributed to distinct phonon correlation lengths, which in turn, were estimated for few-layers GaS.

Experimental Details. Few-layer GaS were obtained by standard mechanical exfoliation[46] from single-crystal sources (provided by *2D semiconductors*) and deposited on thin glass coverslips. The sample thicknesses were estimated by optical contrast, Raman spectroscopy, and atomic force microscopy (AFM).

TERS was performed using a home-built experimental setup described in detail elsewhere.[47] Briefly, it is composed of an optical system based on an inverted microscope, equipped with an X,Y-scan stage, a radially polarized laser beam of 1.96 eV excitation energy and a home-built AFM scan-head, working in a shear-force configuration. The optical and AFM systems are coupled via a gold plasmon-tuned tip pyramid (PTTP)[48] probe, a highly efficient optical nanoantenna capable of making use of the near field information, leading to the tip-enhanced Raman scattering effect. The laser power was adjusted to 225 μW to avoid PTTP damaging and sample heating effects while maintaining a usable signal-to-noise ratio.

Here we used two different gold PTTPs to perform the TERS experiments in GaS. Their apex diameters, directly related to the TERS image resolution, were estimated by scanning electron microscopy (SEM) images and/or by the TERS intensity profiles, and the specific value will be displayed along with the results.

Results and Discussion. Bulk GaS belongs to space group D_{6h}^4, while the monolayer belongs to D_{3h}^1.[49,50] In bulk form, each unit cell is composed by two monolayers (S−Ga−Ga−S), resulting in 24 normal modes at the center of the Brillouin zone. However, only 10 of theses modes are Raman active: $2A_{1g}$, $2E_{2g}$, $2E_{1g}$. The E_{1g} and E_{2g} modes are doubly degenerate with in-plane vibrations, while the modes A_{1g} are out-of-plane vibrations.[50−53] These modes have frequencies (at room temperature and ambient pressure conditions) located at 22.8 cm^{-1} (E_{2g}^2), 74.7 cm^{-1} (E_{1g}^1), 189 cm^{-1} (A_{1g}^1), 291.8 cm^{-1} (E_{1g}^2), 295.8 cm^{-1} (E_{2g}^1), and 360.9 cm^{-1} (A_{1g}^2).[51,53] Here we focus on the most intense A_{1g}^1 and A_{1g}^2 totally symmetric modes. The E_{1g}^2 and E_{2g}^1 modes exhibit similar frequencies and are very low in intensity,[54] which makes the analysis difficult, especially when the GaS thickness is reduced.

Figure 1 shows a far-field Raman map of the A_{1g}^1 mode of a GaS flake, with different numbers of layers. The thicknesses

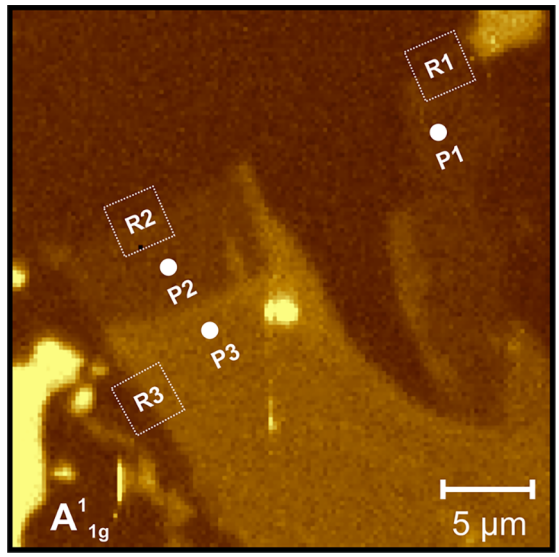

Figure 1. Far-field Raman map of the A_{1g}^1 mode of a GaS flake with different thicknesses. The small dashed-line squared areas set out the regions were the AFM images from Figure 2 were carried out, while the white dots mark the positions were the spectra from Figure 3 were acquired.

were estimated via our home-built AFM scan-head at three small areas on the borders of the GaS flake (see Figure 2), marked with the small dashed-line squares in Figure 1. These three regions, labeled as R1, R2, and R3, have heights of about 1.0, 2.7, and 4.4 nm, respectively. On the basis of these heights, we assigned the three samples as one-layer, three-layer, and five-layer GaS.

We acquired Raman spectra with (TERS) and without (confocal) the presence of the tip at three different positions (see P1, P2, and P3 in Figure 1, and the respective spectra in Figure 3a,c,e). After background subtraction, each A_{1g} Raman peak was fitted with one Lorentzian function (see Figure 3b,d,f) and peak parameters were compared (see Figure 4a). For these analyses, the same PTTP probe was utilized, with an apex diameter of ∼20 nm, estimated via SEM imaging.

As expected, the spectral signal intensity decreases along with the thickness (compare panels a, c, and e in Figure 3). However, the A_{1g}^1 mode is always more enhanced than the A_{1g}^2 mode after approaching the tip, independently of the number of layers, as shown in Figure 3. The spectral enhancement is given by

$$F_{\mathrm{TERS}} = \frac{I_{\mathrm{FF}} + I_{\mathrm{NF}}}{I_{\mathrm{FF}}} = \frac{I_{\mathrm{tip\text{-}down}}}{I_{\mathrm{tip\text{-}up}}} \quad (1)$$

were I_{FF} and I_{NF} denote the far-field (confocal) and near-field (TERS) intensities, respectively. These enhancements are displayed in Figure 3a,c,e for the two totally symmetric modes. For completeness, we also plot F_{TERS} for the E_{2g}^1 mode for five-layer GaS in (e), for the case when this weak peak exhibits reasonable intensity. Besides, our findings show a decreasing (increasing) in A_{1g} frequencies (fwhm) mode with decreasing thickness (Figure 4a), although much less pronounced for the A_{1g}^2 mode, consistent with the results of the refs 12 and 55.

The phonon lifetime (Γ_c) and correlation length (L_c) are related, and their magnitudes can be reduced through phonon scattering by defects and electron−phonon and phonon−phonon interactions. For GaS in the bulk form, a considerable

DOI: 10.1021/acs.nanolett.9b02974
Nano Lett. 2019, 19, 7357−7364

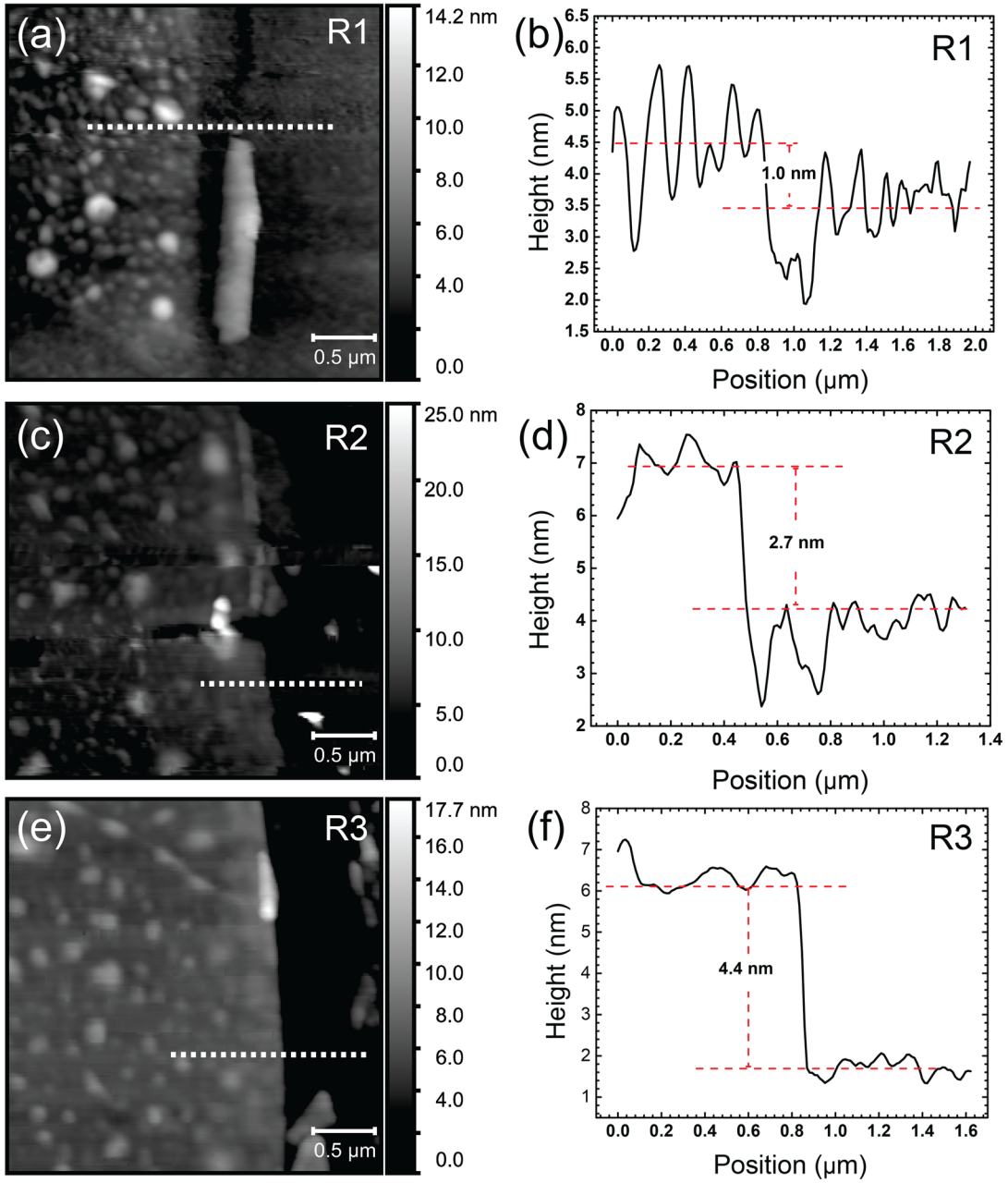

Figure 2. Topographic AFM images recorded in the dashed-line squared areas in Figure 1, in shear-force mode, by using our home-built AFM. (b), (d), (f) are line profiles from the white dashed lines in (a), (c), (e), respectively.

third-order phonon−phonon coupling effect for the A^2_{1g} mode compared to A^1_{1g} was observed in temperature-dependent Raman experiments.[51] These anharmonicity differences are also reflected in the phonon lifetime, which affects the phonon line width, considering Heisenberg time−energy uncertainty relation.

The near-field Raman signal intensity $I_\Gamma^{TERS}(z)$ depends on sample, tip, and instrumental aspects (see eq 2). The sample aspects are the vibrational mode phonon symmetry Γ and the phonon coherence length L_c. The tip aspects are the tip radius r_{tip} and the TERS enhancement factor f_e, where the latter is dependent on plasmonic properties of the tip.[36] The higher the TERS field enhancement (f_e), the steeper the spectral enhancement during a tip−sample approach curve. The instrumental aspects are z_0, the smallest tip−sample separation distance defined by the AFM feedback control, and the constant C_Γ that appears in eq 2. Although C_Γ accounts for the Raman cross section of the Γ symmetry mode (a sample's intrinsic property), it is highly dependent on instrumental factors such as detectors sensitivity, laser intensity, scattering solid angle of collection and system alignment.

Since the two A_{1g} modes display the same symmetry, the differences in phonon anharmonicity should be responsible for their distinct TERS enhancement. Qualitatively, the A^2_{1g} mode exhibits a higher third-order phonon−phonon coupling and, consequently, a lower L_c, which result in lower near-field enhancement as compared to the A^1_{1g} mode, consistent with our results.

Quantitatively, an analysis of the L_c can be done by measuring the Raman spectra as a function of tip−sample distance, as previously reported in graphene[36,44,56] and fully described in ref 57. Since the TERS signal is more intense in

DOI: 10.1021/acs.nanolett.9b02974
Nano Lett. 2019, 19, 7357−7364

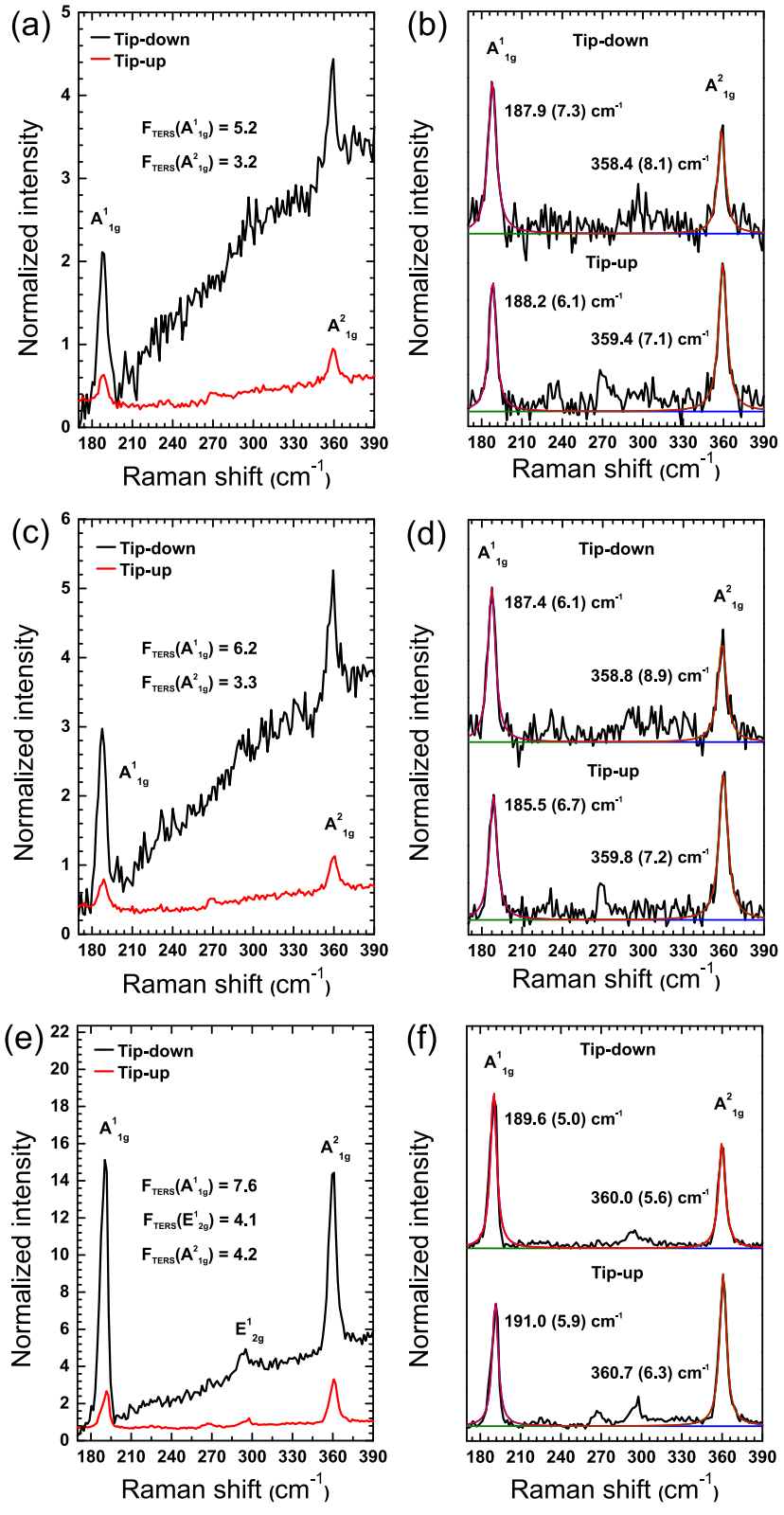

Figure 3. (a), (c), (e) Raman spectra recorded with tip-down (black) and tip-up (red) configurations, acquired at positions P1, P2, and P3 in Figure 1, respectively. The far-field spectra were recorded with 360 s and 10 accumulations, while the near-field spectra were acquired with 60 s and 10 accumulations. (b), (d), (f) Deconvolution of spectra in (a), (c), (e), respectively. Each peak was fitted with one Lorentzian after removing the background, and the peak frequencies and the full width at half-maximum (fwhm) are displayed in cm^{-1}, with the latter given in parentheses. Spectra in (a), (c), (e) are normalized by their accumulation times. Spectra in (b), (d), (f) are normalized by their maximum intensities.

the P3 position, we performed such analysis in P3 using the same TERS tip.

Figures 5a and b show the approach curves for both A^1_{1g} (opened square) and A^2_{1g} (red circle) modes, respectively. The

DOI: 10.1021/acs.nanolett.9b02974
Nano Lett. 2019, 19, 7357−7364

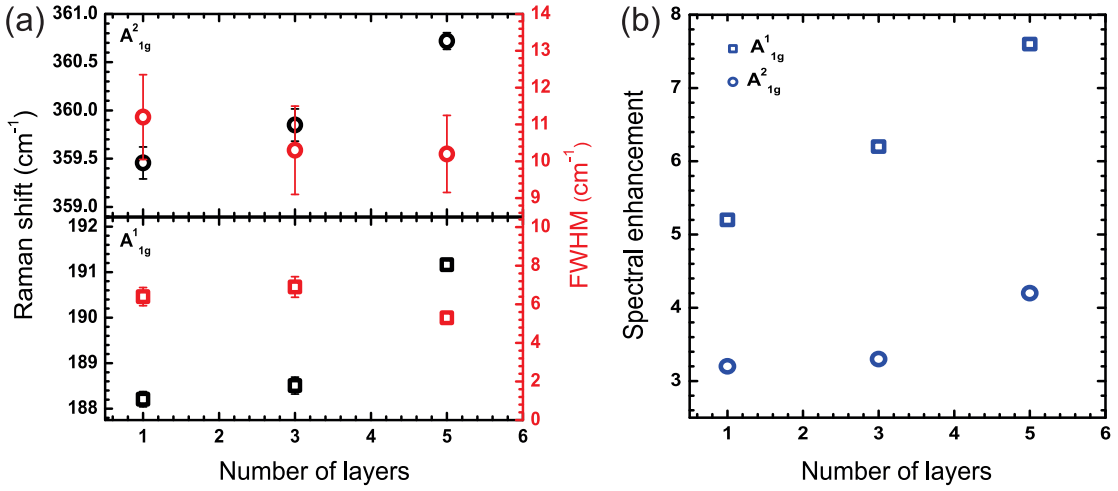

Figure 4. (a) Number of layer dependence of the Raman shift (left axis) and full width at half-maximum (right axis) for the A^1_{1g} (bottom) and A^2_{1g} (top) Raman peaks. (b) Thickness dependence of the TERS spectral enhancement for the A^1_{1g} (empty squares) and the A^2_{1g} (empty circles) modes in GaS.

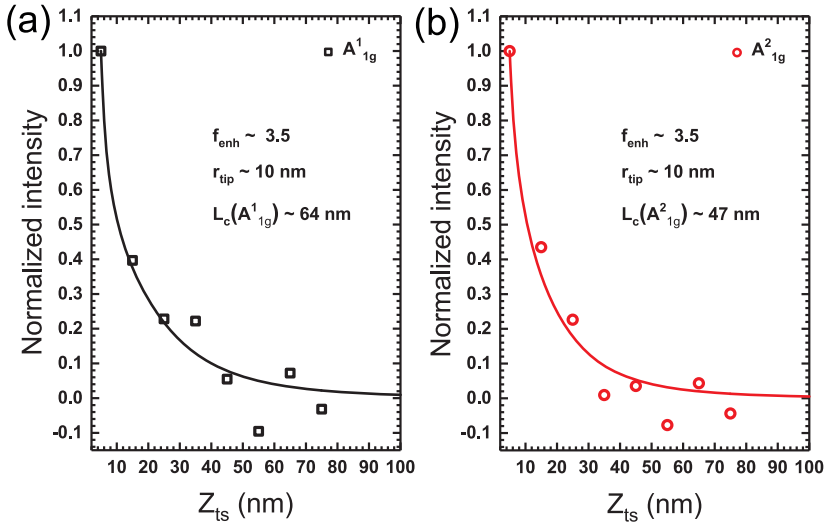

Figure 5. Normalized tip−sample distance dependence, Z_{ts}, for (a) A^1_{1g} (empty black squares) and (b) A^2_{1g} (empty red circles). The black and red curves are the theoretical dependence of Z_{ts} for A^1_{1g} and A^2_{1g} modes, respectively, calculated through eq 2. The output parameters calculated by eq 2 are shown in the graphs.

data were subtracted by the far-field intensity and rescaled so that the near-field values are in units that reproduce the same type of analysis performed in refs 36, 44, and 57. The approach curves show different tip−sample distance dependencies, where the A^2_{1g} mode is steeper, fully consistent with the higher overall enhancement (7.6 against 4.2), suggesting that the A_{1g} modes in GaS have different L_c. In order to extract the L_c parameter from the TERS experiment, the tip-approach data from Figure 5 were fitted using the following relation

$$I_\Gamma^{TERS}(z) = C_\Gamma\left[f_e^4 r_{tip}^{12} g_\Gamma^{TST}(L_c,z) + f_e^2 r_{tip}^6 g_\Gamma^{ST}(L_c,z) + f_e^2 r_{tip}^6 g_\Gamma^{TS}(L_c,z)\right] \quad (2)$$

which expresses the intensity I_Γ^{TERS} measured by TERS as a function of the tip−sample displacement z, for a phonon with symmetry Γ and coherence length L_c, and a tip with field enhancement factor f_e and radius r_{tip}. The functions g^{TST}, g^{ST}, and g^{TS} are related to the scattering modes TST, ST, and TS, which account for the tip−sample−tip, tip−sample, and sample−tip sequences of electromagnetic field interactions, respectively.[44,58] Equation 2 is a simplified version of what has been introduced in refs 44 and 57 with the addition of the TS term. The resulting fitting parameters for the experimental data are $f_e \sim 3.5$, $L_c \approx 64$ nm, and ≈ 47 nm for A^1_{1g} and A^2_{1g}, respectively. To base our finding on solid ground, we performed a second experiment in the P3 location using a different PTTP probe ($r_{tip} \sim 10$, $f_e \sim 2$). The fitting process (not shown) revealed $L_c \approx 60$ nm and ≈ 52 nm for A^1_{1g} and A^2_{1g}, respectively, consistent with the previous experiment, indicating that the results are reproducible.

Finally, we check whether these results are sensitive to the number of GaS layers. Figure 4b displays the totally symmetric spectral mode enhancements obtained at points P1, P2, and P3 in Figure 1, which are assigned as one-layer, three-layer, and five-layer samples. The A^1_{1g} enhancement is always superior to the A^2_{1g}, as already stated, but the spectral enhancements decrease by decreasing the number of layers. Considering eq 1, we expect the I_{FF} to scale linearly with the number of layers (in the few-layer limit) and I_{NF} to exhibit a smaller increase or

DOI: 10.1021/acs.nanolett.9b02974
Nano Lett. 2019, 19, 7357−7364

even to decrease, for two reasons. First, when the tip approaches the GaS surface, the extra layers in the many-layer sample are always more distant from the tip. The second reason would be related to the geometry of our setup.[47] The measurements were performed in an inverted microscope, in which the sample is illuminated from the bottom using a high numerical aperture objective lens. The tip is positioned right above the sample surface, and the collection of the scattered field is made by the same objective positioned at the bottom. In this configuration, the incident field that reaches the tip and scattered field from the tip are both partially absorbed by the sample. Since the GaS flake absorbs more light as the number of layers increase, the influence of the tip should decrease as the sample becomes thicker. Consequently, we conclude that the increase in spectral enhancement when increasing the number of layers has to be due to an increase in L_c. This assumption is reasonable considering the limitation on phonon lifetime to be related to scattering with the surface roughness. Our results are also consistent with the fwhm values reported in Figure 3, since their values decrease with increasing the number of layers.

Conclusion. In summary, we performed a TERS study in order to measure the spatial correlation length of few-layer GaS. Distinct L_c values were found for the A^1_{1g} and A^2_{1g} modes and the distinction is attributed to differences in the phonon anharmonicity of these modes.[51] Unlike graphene, where the mode symmetry is responsible for the differences in TERS intensities, in GaS the different TERS enhancements allow us to access the differences in phonon coherence lengths L_c. The higher the L_c, the higher the TERS enhancement, providing L_c = (62 ± 2) nm and (50 ± 3) nm for A^1_{1g} and A^2_{1g} GaS vibrational modes, respectively. These L_c values were found for five-layer GaS, and our results for three-layer and one-layer GaS indicate L_c decreases with the decreasing number of layers due to scattering with the surface roughness. Our results are of particular importance for GaS-based electronics, and they consolidate a new protocol for TERS applications, where phonon coherence lengths can be obtained optically.

AUTHOR INFORMATION

Corresponding Authors

*E-mail: rsalencar@ufpa.br.

*E-mail: adojorio@fisica.ufmg.br.

ORCID

R. S. Alencar: 0000-0002-9992-7564

Jenaina Ribeiro-Soares: 0000-0001-9248-2243

Notes

The authors declare no competing financial interest.

ACKNOWLEDGMENTS

R.S.A. acknowledges the supports from CNPq/Brazil (grant 150379/2017-0) and from CAPES/Brazil (grant No. 88887.162565/2018-00). H.L.S.M. acknowledges the support from CNPq/Brazil (grant 153532/2016-5). L.G.C. acknowledges CNPq, FAPEMIG, and INCT Nanocarbono. We thank the Brazilian National Council for Scientific and Technological Development (CNPq; Grants No. 310813/2017-4 and No. 433027/2018-5), the Foundation for Research Support of Minas Gerais (Fapemig; Grants No. CEX-APQ-01865-17, No. TEC-AUC-00026-16, No. RED-00185-16, No. RED-00282-16), the Agency for Financing Studies and Projects [FINEP; Grants No. 0501/16 (NANO) from FINEP 02/2014, and FINEP 02/2016] and INMETRO. J.R.-S. acknowledges support from the Pró-Reitoria de Pesquisa and Pró-Reitoria de Gestão (UFLA), and the L'Oréal-UNESCO-Academia Brasileira de Ciências Prêmio Para Mulheres na Ciência (Prize for Women in Science; Brazil, 2017). A.G.S.F. acknowledge financial support from CNPq (Grants No. 438144/2018-0 and No. 309309/2017-4) agency.

REFERENCES

(1) Li, X.-L.; Han, W.-P.; Wu, J.-B.; Qiao, X.-F.; Zhang, J.; Tan, P.-H. Layer-Number Dependent Optical Properties of 2D Materials and their Application for Thickness Determination. *Adv. Funct. Mater.* **2017**, *27*, 1604468.

(2) Gupta, A.; Sakthivel, T.; Seal, S. Recent Development in 2D Materials Beyond Graphene. *Prog. Mater. Sci.* **2015**, *73*, 44−126.

(3) Hu, P.; Wang, L.; Yoon, M.; Zhang, J.; Feng, W.; Wang, X.; Wen, Z.; Idrobo, J. C.; Miyamoto, Y.; Geohegan, D. B.; Xiao, K. Highly Responsive Ultrathin GaS Nanosheet Photodetectors on Rigid and Flexible Substrates. *Nano Lett.* **2013**, *13*, 1649−1654.

(4) Xu, M.; Liang, T.; Shi, M.; Chen, H. Graphene-Like Two-Dimensional Materials. *Chem. Rev.* **2013**, *113*, 3766−3798.

(5) Yang, S.; Li, Y.; Wang, X.; Huo, N.; Xia, J.-B.; Li, S.-S.; Li, J. High Performance Few-Layer GaS Photodetector and its Unique Photo-Response in Different Gas Environments. *Nanoscale* **2014**, *6*, 2582−2587.

(6) Jung, C. S.; Shojaei, F.; Park, K.; Oh, J. Y.; Im, H. S.; Jang, D. M.; Park, J.; Kang, H. S. Red-to-Ultraviolet Emission Tuning of Two-Dimensional Gallium Sulfide/Selenide. *ACS Nano* **2015**, *9*, 9585−9593.

(7) Shen, G.; Chen, D.; Chen, P.-C.; Zhou, C. Vapor-Solid Growth of One-Dimensional Layer-Structured Gallium Sulfide Nanostructures. *ACS Nano* **2009**, *3*, 1115−1120.

(8) Steiner, M.; Freitag, M.; Perebeinos, V.; Tsang, J. C.; Small, J. P.; Kinoshita, M.; Yuan, D.; Liu, J.; Avouris, P. Phonon Populations and Electrical Power Dissipation in Carbon Nanotube Transistors. *Nat. Nanotechnol.* **2009**, *4*, 320−324.

(9) Berciaud, S.; Han, M. Y.; Mak, K. F.; Brus, L. E.; Kim, P.; Heinz, T. F. Electron and Optical Phonon Temperatures in Electrically Biased Graphene. *Phys. Rev. Lett.* **2010**, *104*, 227401.

(10) Tian, Z.; Esfarjani, K.; Shiomi, J.; Henry, A. S.; Chen, G. On the Importance of Optical Phonons to Thermal Conductivity in Nanostructures. *Appl. Phys. Lett.* **2011**, *99*, 053122.

(11) Xie, G.; Ding, D.; Zhang, G. Phonon Coherence and its Effect on Thermal Conductivity of Nanostructures. *Advances in Physics: X* **2018**, *3*, 1480417.

(12) Late, D. J.; Liu, B.; Matte, H. S. S. R.; Rao, C. N. R.; Dravid, V. P. Rapid Characterization of Ultrathin Layers of Chalcogenides on SiO_2/Si Substrates. *Adv. Funct. Mater.* **2012**, *22*, 1894−1905.

(13) Late, D. J.; Liu, B.; Luo, J.; Yan, A.; Matte, H. S. S. R.; Grayson, M.; Rao, C. N. R.; Dravid, V. P. GaS and GaSe Ultrathin Layer Transistors. *Adv. Mater.* **2012**, *24*, 3549−3554.

(14) Cançado, L. G.; da Silva, M. G.; Ferreira, E. H. M.; Hof, F.; Kampioti, K.; Huang, K.; Pénicaud, A.; Achete, C. A.; Capaz, R. B.; Jorio, A. Disentangling Contributions of Point and Line Defects in the Raman Spectra of Graphene-Related Materials. *2D Mater.* **2017**, *4*, 025039.

(15) Mignuzzi, S.; Pollard, A. J.; Bonini, N.; Brennan, B.; Gilmore, I. S.; Pimenta, M. A.; Richards, D.; Roy, D. Effect of Disorder on Raman Scattering of Single-Layer MoS_2. *Phys. Rev. B: Condens. Matter Mater. Phys.* **2015**, *91*, 195411.

(16) Rogalski, J.; Braun, K.; Horneber, A.; van den Berg, M.; Uihlein, J.; Peisert, H.; Chassé, T.; Meixner, A. J.; Zhang, D. STM Tip-Enhanced Raman Spectroscopy and the Investigation of Doped Graphene. *Vib. Spectrosc.* **2017**, *91*, 128−135 Prominent Young Vibrational Spectroscopists .

(17) Das, A.; Pisana, S.; Chakraborty, B.; Piscanec, S.; Saha, S. K.; Waghmare, U. V.; Novoselov, K. S.; Krishnamurthy, H. R.; Geim, A. K.; Ferrari, A. C.; Sood, A. K. Monitoring Dopants by Raman

DOI: 10.1021/acs.nanolett.9b02974
Nano Lett. 2019, 19, 7357−7364

Scattering in an Electrochemically Top-Gated Graphene Transistor. *Nat. Nanotechnol.* **2008**, *3*, 210.
(18) Chakraborty, B.; Bera, A.; Muthu, D. V. S.; Bhowmick, S.; Waghmare, U. V.; Sood, A. K. Symmetry-Dependent Phonon Renormalization in Monolayer MoS_2 Transistor. *Phys. Rev. B: Condens. Matter Mater. Phys.* **2012**, *85*, 161403.
(19) Ranjan, P.; Sahu, T. K.; Bhushan, R.; Yamijala, S. S.; Late, D. J.; Kumar, P.; Vinu, A. Freestanding Borophene and its Hybrids. *Adv. Mater.* **2019**, *31*, 1900353.
(20) Alencar, R. S.; Saboia, K. D. A.; Machon, D.; Montagnac, G.; Meunier, V.; Ferreira, O. P.; San-Miguel, A.; Souza Filho, A. G. Atomic-Layered MoS_2 on SiO_2 Under High Pressure: Bimodal Adhesion and Biaxial Strain Effects. *Phys. Rev. Materials* **2017**, *1*, 024002.
(21) Machon, D.; Bousige, C.; Alencar, R.; Torres-Dias, A.; Balima, F.; Nicolle, J.; de Sousa Pinheiro, G.; Souza Filho, A. G.; San-Miguel, A. Raman Scattering Studies of Graphene under High Pressure. *J. Raman Spectrosc.* **2018**, *49*, 121−129.
(22) Zabel, J.; Nair, R. R.; Ott, A.; Georgiou, T.; Geim, A. K.; Novoselov, K. S.; Casiraghi, C. Raman Spectroscopy of Graphene and Bilayer under Biaxial Strain: Bubbles and Balloons. *Nano Lett.* **2012**, *12*, 617−621.
(23) Pawbake, A.; Bellin, C.; Paulatto, L.; Béneut, K.; Biscaras, J.; Narayana, C.; Late, D. J.; Shukla, A. Pressure-Induced Phase Transitions in Germanium Telluride: Raman Signatures of Anharmonicity and Oxidation. *Phys. Rev. Lett.* **2019**, *122*, 145701.
(24) Late, D. J. Temperature-Dependent Phonon Shifts in Atomically Thin $MoTe_2$ Nanosheets. *Applied Materials Today* **2016**, *5*, 98−102.
(25) Pawbake, A. S.; Pawar, M. S.; Jadkar, S. R.; Late, D. J. Large Area Chemical Vapor Deposition of Monolayer Transition Metal Dichalcogenides and their Temperature Dependent Raman Spectroscopy Studies. *Nanoscale* **2016**, *8*, 3008−3018.
(26) Verma, P. Tip-Enhanced Raman Spectroscopy: Technique and Recent Advances. *Chem. Rev.* **2017**, *117*, 6447−6466.
(27) Stöckle, R. M.; Suh, Y. D.; Deckert, V.; Zenobi, R. Nanoscale Chemical Analysis by Tip-Enhanced Raman Spectroscopy. *Chem. Phys. Lett.* **2000**, *318*, 131−136.
(28) Bao, W.; Borys, N. J.; Ko, C.; Suh, J.; Fan, W.; Thron, A.; Zhang, Y.; Buyanin, A.; Zhang, J.; Cabrini, S.; Ashby, P. D.; Weber-Bargioni, A.; Tongay, S.; Aloni, S.; Ogletree, D. F.; Wu, J.; Salmeron, M. B.; Schuck, P. J. Visualizing Nanoscale Excitonic Relaxation Properties of Disordered Edges and Grain Boundaries in Monolayer Molybdenum Disulfide. *Nat. Commun.* **2015**, *6*, 7993.
(29) Park, K.-D.; Khatib, O.; Kravtsov, V.; Clark, G.; Xu, X.; Raschke, M. B. Hybrid Tip-Enhanced Nanospectroscopy and Nanoimaging of Monolayer WSe_2 with Local Strain Control. *Nano Lett.* **2016**, *16*, 2621−2627.
(30) Su, W.; Kumar, N.; Mignuzzi, S.; Crain, J.; Roy, D. a. Nanoscale Mapping of Excitonic Processes in Single-Layer MoS_2 Using Tip-Enhanced Photoluminescence Microscopy. *Nanoscale* **2016**, *8*, 10564−10569.
(31) Lee, C.; Jeong, B. G.; Yun, S. J.; Lee, Y. H.; Lee, S. M.; Jeong, M. S. Unveiling Defect-Related Raman Mode of Monolayer WS_2 via Tip-Enhanced Resonance Raman Scattering. *ACS Nano* **2018**, *12*, 9982−9990.
(32) Tang, C.; He, Z.; Chen, W.; Jia, S.; Lou, J.; Voronine, D. V. Quantum Plasmonic Hot-Electron Injection in Lateral $WSe_2/MoSe_2$ Heterostructures. *Phys. Rev. B: Condens. Matter Mater. Phys.* **2018**, *98*, 041402.
(33) Park, K.-D.; Raschke, M. B.; Atkin, J. M.; Lee, Y. H.; Jeong, M. S. Probing Bilayer Grain Boundaries in Large-Area Graphene with Tip-Enhanced Raman Spectroscopy. *Adv. Mater.* **2017**, *29*, 1603601.
(34) Su, W.; Kumar, N.; Dai, N.; Roy, D. Nanoscale Mapping of Intrinsic Defects in Single-Layer Graphene Using Tip-Enhanced Raman Spectroscopy. *Chem. Commun.* **2016**, *52*, 8227−8230.
(35) Beams, R.; Cançado, L. G.; Jorio, A.; Vamivakas, A. N.; Novotny, L. Tip-Enhanced Raman Mapping of Local Strain in Graphene. *Nanotechnology* **2015**, *26*, 175702.
(36) Beams, R.; Cançado, L. G.; Oh, S.-H.; Jorio, A.; Novotny, L. Spatial Coherence in Near-Field Raman Scattering. *Phys. Rev. Lett.* **2014**, *113*, 186101.
(37) Campos, J. a. L. E.; Miranda, H.; Rabelo, C.; Sandoz-Rosado, E.; Pandey, S.; Riikonen, J.; Cano-Marquez, A. G.; Jorio, A. Applications of Raman Spectroscopy in Graphene-Related Materials and the Development of Parameterized PCA for Large-Scale Data Analysis. *J. Raman Spectrosc.* **2018**, *49*, 54−65.
(38) Stadler, J.; Schmid, T.; Zenobi, R. Nanoscale Chemical Imaging of Single-Layer Graphene. *ACS Nano* **2011**, *5*, 8442−8448.
(39) Rickman, R. H.; Dunstan, P. R. Enhancement of Lattice Defect Signatures in Graphene and Ultrathin Graphite Using Tip-Enhanced Raman Spectroscopy. *J. Raman Spectrosc.* **2014**, *45*, 15−21.
(40) Vantasin, S.; Tanaka, Y.; Uemura, S.; Suzuki, T.; Kutsuma, Y.; Doujima, D.; Kaneko, T.; Ozaki, Y. Characterization of SiC-Grown Epitaxial Graphene Microislands Using Tip-Enhanced Raman Spectroscopy. *Phys. Chem. Chem. Phys.* **2015**, *17*, 28993−28999.
(41) Vantasin, S.; Tanabe, I.; Tanaka, Y.; Itoh, T.; Suzuki, T.; Kutsuma, Y.; Ashida, K.; Kaneko, T.; Ozaki, Y. Tip-Enhanced Raman Scattering of the Local Nanostructure of Epitaxial Graphene Grown on 4H-SiC (0001). *J. Phys. Chem. C* **2014**, *118*, 25809−25815.
(42) Suzuki, T.; Itoh, T.; Vantasin, S.; Minami, S.; Kutsuma, Y.; Ashida, K.; Kaneko, T.-a.; Morisawa, Y.; Miura, T.; Ozaki, Y. Tip-Enhanced Raman Spectroscopic Measurement of Stress Change in the Local Domain of Epitaxial Graphene on the Carbon Face of 4H-SiC(000−1). *Phys. Chem. Chem. Phys.* **2014**, *16*, 20236−20240.
(43) Snitka, V.; Rodrigues, R. D.; Lendraitis, V. Novel Gold Cantilever for Nano-Raman Spectroscopy of Graphene. *Microelectron. Eng.* **2011**, *88*, 2759−2762 Proceedings of the 36th International Conference on Micro- and Nano-Engineering (MNE) .
(44) Cançado, L. G.; Beams, R.; Jorio, A.; Novotny, L. Theory of Spatial Coherence in Near-Field Raman Scattering. *Phys. Rev. X* **2014**, *4*, 031054.
(45) Maximiano, R. V.; Beams, R.; Novotny, L.; Jorio, A.; Cançado, L. G. Mechanism of Near-Field Raman Enhancement in Two-Dimensional Systems. *Phys. Rev. B: Condens. Matter Mater. Phys.* **2012**, *85*, 235434.
(46) Novoselov, K. S.; Neto, A. H. C. Two-Dimensional Crystals-Based Heterostructures: Materials with Tailored Properties. *Phys. Scr.* **2012**, *2012*, 014006.
(47) Cançado, L. G.; Hartschuh, A.; Novotny, L. Tip-Enhanced Raman Spectroscopy of Carbon Nanotubes. *J. Raman Spectrosc.* **2009**, *40*, 1420−1426.
(48) Vasconcelos, T. L.; Archanjo, B. S.; Oliveira, B. S.; Valaski, R.; Cordeiro, R. C.; Medeiros, H. G.; Rabelo, C.; Ribeiro, A.; Ercius, P.; Achete, C. A.; Jorio, A.; Cançado, L. G. Plasmon-Tunable Tip Pyramids: Monopole Nanoantennas for Near-Field Scanning Optical Microscopy. *Adv. Opt. Mater.* **2018**, *6*, 1800528.
(49) van der Ziel, J.; Meixner, A.; Kasper, H. Raman Scattering From β-GaS. *Solid State Commun.* **1973**, *12*, 1213−1215.
(50) Dzhakhangirli, Z. A. First-Principles Investigation of the Phonon Spectrum of β-GaS. *Phys. Solid State* **2012**, *54*, 1092−1095.
(51) Gasanly, N.; Aydinli, A.; Özkan, H.; Kocabas, C. Temperature Dependence of the First-Order Raman Scattering in GaS Layered Crystals. *Solid State Commun.* **2000**, *116*, 147−151.
(52) Cingolani, A.; Lugarà, M.; Scamarcio, G.; Lévy, F. Raman Spectroscopy in GaS: Zone Boundary Phonon Interactions. *Nuovo Cimento Soc. Ital. Fis., D* **1989**, *11*, 455−466.
(53) van der Ziel, J.; Meixner, A.; Kasper, H. Raman Scattering from β-GaS. *Solid State Commun.* **1973**, *12*, 1213−1215.
(54) Zhang, X.; Tan, Q.-H.; Wu, J.-B.; Shi, W.; Tan, P.-H. Review on the Raman Spectroscopy of Different Types of Layered Materials. *Nanoscale* **2016**, *8*, 6435−6450.
(55) Jastrzebski, C.; Olkowska, K.; Jastrzebski, D. J.; Wierzbicki, M.; Gebicki, W.; Podsiadlo, S. Raman Scattering Studies on very Thin Layers of Gallium Sulfide (GaS) as a Function of Sample Thickness and Temperature. *J. Phys.: Condens. Matter* **2019**, *31*, 075303.
(56) Pfeiffer, M.; Senkovskiy, B. V.; Haberer, D.; Fischer, F. R.; Yang, F.; Meerholz, K.; Ando, Y.; Grüneis, A.; Lindfors, K. Enhanced

DOI: 10.1021/acs.nanolett.9b02974
Nano Lett. 2019, 19, 7357−7364

Light−Matter Interaction of Aligned Armchair Graphene Nanoribbons Using Arrays of Plasmonic Nanoantennas. *2D Mater.* **2018**, *5*, 045006.
(57) Ribeiro Neto, A.; Rabelo, C.; Cancado, L. G.; Engel, M.; Steiner, M.; Jorio, A. Protocol and Reference Material for Measuring the Nanoantenna Enhancement Factor in Tip-Enhanced Raman Spectroscopy. In *4th International Symposium on Instrumentation Systems, Circuits and Transducers (INSCIT)*; 2019.
(58) Novotny, L.; Hecht, B. *Principles of Nano-Optics*, 2nd ed.; Cambridge University Press: Cambridge, 2012.

DOI: 10.1021/acs.nanolett.9b02974
Nano Lett. 2019, 19, 7357−7364